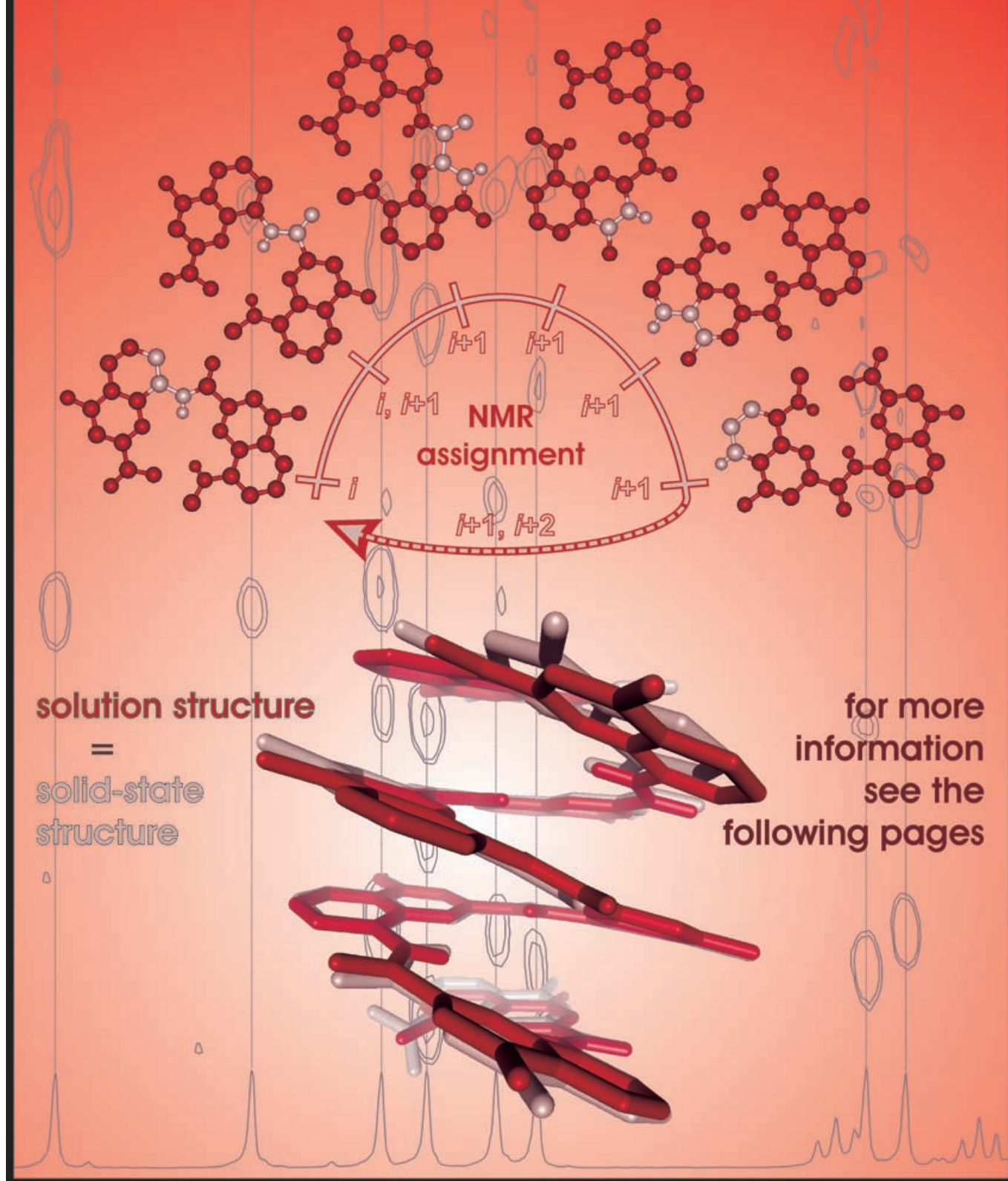


Solution Structure of Aromatic Oligoamide Foldamers



Solution Structure of Quinoline- and Pyridine-Derived Oligoamide Foldamers

Christel Dolain, Axelle Grélard, Michel Laguerre, Hua Jiang, Victor Maurizot, and Ivan Huc*^[a]

Abstract: The unambiguous elucidation of a new folded structure in solution may prove to be a very challenging task. The NMR protocols developed for solving the solution structures of α -peptides have been applied to aliphatic β - and γ -peptides but are not directly applicable to aromatic oligomers. In particular, the string of spin systems in an aromatic sequence cannot be reconstituted solely from correlations between protons. For aromatic oligomers, it is shown that the assignment of a

large part of the ^{13}C NMR spectrum through HMBC and HSQC experiments allows to unambiguously assign proton NMR spectra and in turn to interpret NOE correlations. This has been implemented both with quinoline- and pyridine-derived oligoamide fol-

damers, and should be applicable to a wide range of oligomers including various combinations of monomers. The NOE correlations allow the unambiguous solution structure elucidation of helical conformations of oligoamides derived from pyridine and quinoline monomers showing that, in these series, the solution structures correspond very well to the structures observed in the solid state.

Keywords: conformation analysis • helical structures • molecular dynamics • NMR spectroscopy • supra-molecular chemistry

Introduction

Over the last decade, intense efforts have been devoted to the design, synthesis and structural studies of foldamers—artificial oligomers that adopt well defined folded conformations in solution, mimicking the folded structures of biopolymers.^[1,2] Foldamers provide a broader context from which to view biopolymer structures. It has been shown that the secondary helical and linear motifs of proteins are not restricted to the α -peptide backbone but belong to many classes of oligomers as, for example, aliphatic β -, γ -, and δ -peptides.^[2] Interest for these new molecules stems largely from the hope that they may mimic not only biological structures but

also biological functions. Some show promising biological activities^[2,3] and others have found applications in molecular recognition.^[4-7]

Judging by the rapidly increasing number of new foldamer families that are being reported, the synthesis of new interesting oligomers does not constitute a major obstacle. However, the unambiguous elucidation of a new folded structure in solution may prove to be a very challenging task. For oligomers bearing chiral groups, circular dichroism may give a hint that a structure is folded, though such data should be handled with great care.^[8] For the so called peptidomimetic backbones, for example, aliphatic β , γ , and δ -peptides, NMR protocols simply derived from those developed to study the structure of α -peptides allow to interpret NMR spectra and resolve solution structures. In particular, NOESY correlations and scalar couplings between amide protons and adjacent aliphatic protons allow to reconstitute the sequence of monomers and fully assign ^1H NMR spectra.^[9] In peptides bearing numerous tetrasubstituted α -carbons, homonuclear scalar correlations can no longer be used for resonance assignment. Heteronuclear multiple bond coherence (HMBC) experiments have then been exploited to perform sequential assignments using interactions of the type $\text{NH}_i \rightarrow \text{CO}_i \rightarrow \text{NH}_{i+1}$.^[10]

[a] Dr. C. Dolain, A. Grélard, Dr. M. Laguerre, Dr. H. Jiang, Dr. V. Maurizot, Dr. I. Huc
Institut Européen de Chimie et Biologie
2 rue Robert Escarpit, 33607 Pessac Cedex (France)
Fax: (+33)540-003-009
E-mail: i.huc@iecb.u-bordeaux.fr

Supporting information for this article is available on the WWW under <http://www.chemeurj.org/> or from the author. COSY NMR spectra of oligomers **1** and **2**, table showing NOE correlations for oligomer **1**, tables showing the resonances of protons and carbons and the HMBC, HSCQ correlations observed between them for oligomers **1** and **2**.

The situation is even more complicated for the many families of foldamers whose backbone strongly differ from biological backbones as those that include numerous aromatic functions. Aromatic ^1H NMR signals often strongly overlap making a direct assignment based on the ^1H NMR spectra difficult if not impossible. Indirect evidence of folding can sometimes be obtained from strong changes in the UV/Vis absorption spectra and fluorescence spectra, as with oligophenylethylenes.^[11] A partial assignment of NMR spectra may allow to identify some NOE correlations and obtain partial, and yet valuable, evidence of folding.^[6,12] However, these difficulties clearly call for the development of new approaches to structural studies of foldamers in solution. An original development was proposed by Moore et al. who introduced two spin labels in an oligophenylethylenylene oligomer and used electron spin resonance spectroscopy to determine the helical pitch of the folded structures.^[13] In the following we wish to report a simple NMR protocol that allowed the complete assignment of ^1H NMR spectra and, to a large extent, of ^{13}C NMR spectra, and the unambiguous solution structure elucidation of helical oligoamides derived from pyridine and quinoline monomers.

Previously, we have reported on the ability of several families of aza-aromatic oligoamides to fold into remarkably stable helices stabilized by intramolecular aromatic–aromatic interactions and by both attractive and repulsive electrostatic interactions involving either the amide hydrogen or oxygen on the one hand, and the adjacent aromatic nitrogen and hydrogen atoms on the other hand.^[1c] We have mainly studied oligoamides of 8-amino-2-quinolinecarboxylic acid,^[14] and oligoamides of 2,6-diaminopyridine and 2,6-pyridinedicarboxylic acids.^[15–17] We also recently started to combine these two series in a single sequence.^[7] The folded structures of these oligomers have been extensively characterized in the solid state by single crystal X-ray crystallography.^[14–16] In solution, however, a number of elements indicate that the same conformations prevail, but this is only supported by indirect evidence. For example, the ^1H NMR spectra are sharp and distributed over a wide range of chemical shifts despite the repetitive nature of the sequences, suggesting different environments of the units; amide protons involved in intramolecular hydrogen bonding are deshielded (signals at 10–12 ppm); increasing strand length results in a strong shielding of aromatic, amide and ester protons that can be attributed to tight contacts between aromatic rings; diastereotopic motifs consistent with the chiral nature of a helix emerge for long oligomers. All these elements are consistent with the assumption that the structures observed in the solid state exist in solution but they do not provide a definite proof.

In the following, we show that the ^1H NMR spectra of these oligomers can be fully assigned using HMBC and HSQC NMR protocols and a relatively standard equipment, that is, a 400 MHz spectrometer with a shielded magnet. Resonance assignment in turn allows for the interpretation of the NOESY correlations and fully solve the solution structure. The strategy followed here represents an extension of

the approach developed for peptides bearing numerous tetrasubstituted α -carbons.^[10] We have used two representative examples in the quinoline and in the pyridine series (structures **1** and **2** in Figure 1). But similar experiments may, in principle, be performed with a wide variety of foldamers bearing aromatic groups.

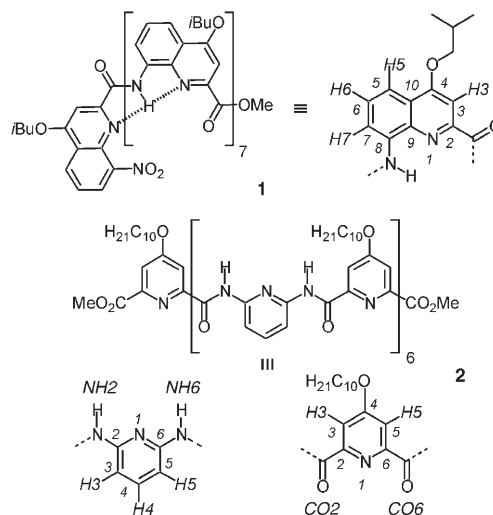


Figure 1. Structures of quinoline derived oligomer **1** and pyridine derived oligomer **2**, and numbering of the aromatic protons and carbons. Monomers are numbered from the N-terminus in **1** and from any terminal ester of oligomer **2** (the central unit is thus ring 7). Protons and carbons are numbered according to their position on the aromatic ring, and to the position of this ring in the sequence. For example, H3-6 corresponds to the proton in position 3 of the sixth unit; CO2-3 corresponds to the carbonyl carbon in position 2 of the third unit.

Results and Discussion

Choice of the oligomeric sequences: Octamer **1** and tridecamer **2** (Figure 1) were selected as representative examples of oligoamides derived from 8-amino-2-quinolinecarboxylic acid and from 2,6-diaminopyridine and 2,6-pyridinedicarboxylic acid, respectively. Their alkyl chains provide high solubility in chlorinated and aromatic solvents. Both oligomers had to be long enough, firstly to make sure that they are well folded, as helix stability increases with length^[14–17] and, secondly, to avoid the dimerization of **2** into double helices which would seriously complicate NMR spectra. Indeed oligomers such as **2** have been shown to hybridize into double helical dimers.^[16,17] But this tends to decrease with oligomer length down to undetectable levels for longer strands.^[17] If necessary, the proportion of double helix may also be reduced upon diluting the sample. On the other hand, the length of both **1** and **2** had to be limited because NMR spectra become more and more complex and signals overlap is problematic as the number of units increases. CDCl_3 was selected because the signals are well spread out in this solvent. This effect is much more pronounced in the quinoline series than in the pyridine series (Figure 2), despite the fact that the pyridine derived oligomers intrinsical-

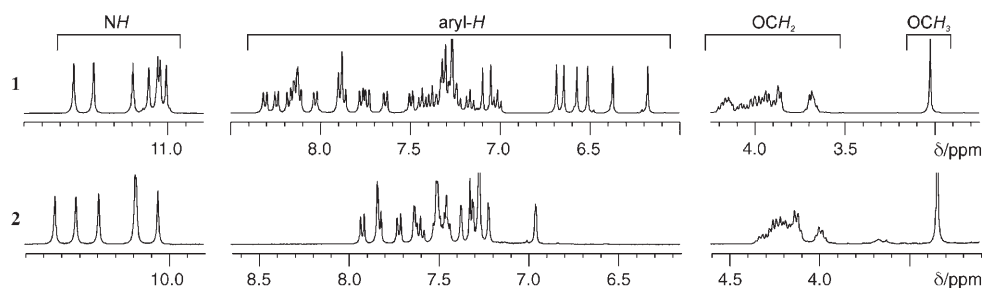


Figure 2. Parts of the 400 MHz ^1H NMR spectra of oligomers **1** and **2** at a concentration of 5 mM and 1 mM, respectively, in CDCl_3 at 300 K showing the amide, aromatic, OCH_2 and OCH_3 resonances. The scales of the two spectra have been adjusted so that the signals of similar protons of each compound coincide.

ly possess two kinds of monomers whereas the quinoline oligomers consist of only one kind of monomer. To limit the number of signals and thus signals overlap in the pyridine series without reducing oligomer length, we decided to use a symmetrical oligomer. Symmetry divides the number of signals per two and leads to an acceptable degree of overlap in **2** (Figure 2, bottom), though it remains more significant than for **1**. As discussed later, symmetry is expected to cause degeneration of the signals and ambiguity in signal assignment. Nevertheless, this complication was preferred to ambiguity arising from signal overlap.

The helical conformation of octamer **1** was previously characterized in the solid state by X-ray crystallography.^[14a] The helical conformations of oligomers such as **2** with up to 11 pyridine rings but no alkoxy substituents were also characterized in the solid state.^[15] As mentioned in the Introduction, evidence exists that these oligomers adopt helical conformations in solution similar to that observed in the solid, but this evidence is only indirect. For example: i) hydrogen-bonded amide protons are deshielded (signals at 11–12 ppm for **1** and 10–11 ppm for **2**); ii) consistent with tight contacts between aromatic rings in the helix, aromatic and ester protons are shielded compared with shorter oligomers. For example, the signal of the methyl ester is found at 3.03 ppm in **1** and 3.34 ppm in **2**, compared with about 4.10 ppm in the corresponding monomers; iii) signals assigned to the OCH_2 groups of the alkoxy side chains at 3.6–4.3 ppm in **1** and 3.9–4.4 ppm in **2** show diastereotopic patterns consistent with the intrinsic chirality of a helical conformation.

Assignment of the spin systems and reconstitution of the sequences: Solution studies were performed to assess directly whether the folded structures observed in the solid state are also prominent in solution. The structures of **1** and **2** were investigated by 1D and 2D NMR spectroscopy in CDCl_3 . Some information stemming from the coupling pattern allows to identify a few signals. For **1**, singlets found between 6.15 and 7.10 ppm belong to aromatic H3, doublets ($J=6.7$ Hz) and triplets ($J=8.0$ Hz) between 7.01 and 8.30 ppm belong to protons H5, H7 and H6. For **2**, sharp doublets ($J=1.3$ Hz) belong to protons H3 and H5 of three of four pyridinedicarbonyl rings; the central ring gives rise to a singlet because protons H3 and H5 are equivalent.

Doublets and triplets belong to protons H3, H5 and H4 of the three diaminopyridine rings.

The spin systems of the different residues of octamer **1** were partially identified from DQF-COSY experiments: strong correlations between H5, H6 and H7 protons of all eight quinoline residues and a few weaker long range correlations between H3 on the one hand and H5, H6 or H7 protons on the other hand allow to regroup most aromatic protons belonging to the same residue.^[18] However, these experiments do not allow to distinguish H5 and H7 protons. The whole spin systems were unambiguously identified from HMBC experiments and required the assignment of the part of the ^{13}C NMR spectrum corresponding to the backbone of octamer **1** (almost 80 carbons). As shown in Figure 3, long-range correlations between protons and carbons H6–C10 (3J), C10–H3 (3J), H3–C4 (2J) and C4–H5 (3J) permit the complete assignment of all spin systems and, at the same time, to differentiate H5 from H7 on each quinoline ring.

For tridecamer **2**, strong DQF-COSY correlations between H3 and H5 protons of pyridinedicarbonyl rings allow to determine all spin systems of these units, though they do not allow to tell which signal corresponds to H3 and which

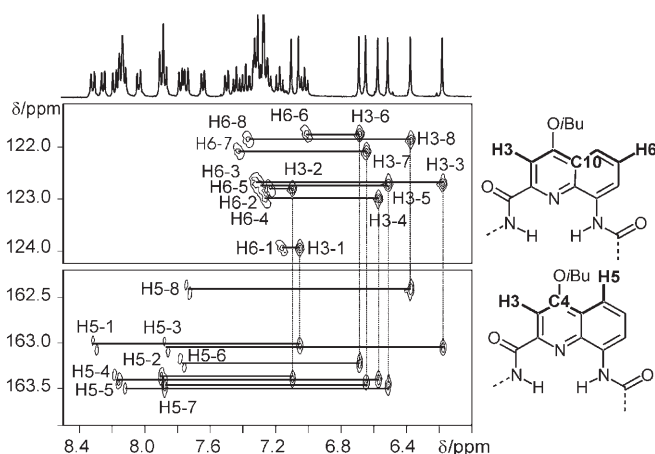


Figure 3. Parts of the 400 MHz HMBC plot of **1** in CDCl_3 at 300 K, showing cross-peaks between protons H3 and H6, and carbon C10 (top) and cross-peaks between protons H3, H5 and carbon C4 (bottom). The horizontal scale is that of proton resonances and the vertical scale is that of carbon resonances.

signal corresponds to H5. On the other hand, the assignment of the spin system of the three different diaminopyridine rings is not unequivocal. Overlap between H3, H4 and H5 protons of diaminopyridine rings leads to less well-defined spin systems of these units, two of them could not be determined unambiguously. The assignment of these spin systems and the distinction between H3 and H5 protons on both diaminopyridine units and pyridinedicarbonyl units could only be achieved during the reconstitution of the whole sequence (see below).

The sequences were assigned on the basis of 2D HMBC, HSQC and 1D ^{13}C experiments. As shown in Figure 4, for octamer **1**, the strong H7–C7 HSQC and C7–NH, NH–CO and CO–H3 HMBC correlations allow to go easily from residue i to residue $i+1$. This assignment is more difficult for tridecamer **2** because of the presence of the two different pyridinedicarbonyl and diaminopyridine units. The numerous correlations necessary to go from residue i to residue $i+1$ and then residue $i+2$ are represented in Figures 5 and 6. Starting from proton H5 of a diaminopyridine unit, correlations H5–C5 (HSQC), C5–NH6 (HMBC), NH6–CO2 (HMBC), and CO2–H3 (HMBC) allow to establish a connection to the adjacent pyridinedicarbonyl ring. Then, correlations H3–C3 (HSQC) and C3–H5 (HMBC) allow to definitely distinguish H3 from H5 on the pyridinedicarbonyl unit. A similar string of correlations allows to connect this H5 proton of a pyridinedicarbonyl unit to the H3 protons of the next diaminopyridine unit: H5–CO6 (HMBC), CO6–NH2 (HMBC), NH2–C3 (HMBC). Finally, correlations C3–H3 (HSQC) and H3–C5 (HMBC) allow to distinguish H3 from H5 on this diaminopyridine unit.

The steps described above allow to shift from one unit to the next in the sequence following well-defined correlations. To fully assign the sequence, an unambiguous starting point is also necessary. A few signals may easily be assigned because the proton or carbons to which they correspond are close to the N- or C-terminal extremities of the strands. Their chemical shifts are noticeably different because of the presence of terminal nitro or methyl ester functions. In octamer **1**, the signal of carbon C8-1 which bears the nitro group is found at 145.0 ppm whilst all other C8 carbons are found between 132.7 and 134.3 ppm. Similarly,

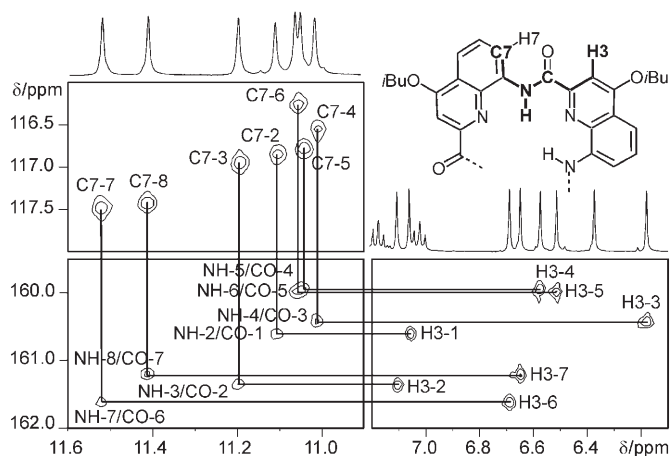


Figure 4. Parts of the 400 MHz HMBC plot of **1** in CDCl_3 at 300 K, showing cross-peaks between carbons C7 and amide protons (top), between amide protons and carbonyl carbons (bottom left), and between carbonyl and H3 protons (bottom right) used for sequence assignment to go from residue i to residue $i+1$. The horizontal scale is that of proton resonances and the vertical scale is that of carbon resonances.

the signal of carbonyl of the ester function CO-8 is found at 164.0 ppm, whilst the signals of amide carbonyls range between 159.9 and 161.6 ppm. In **2**, the signal of the ester

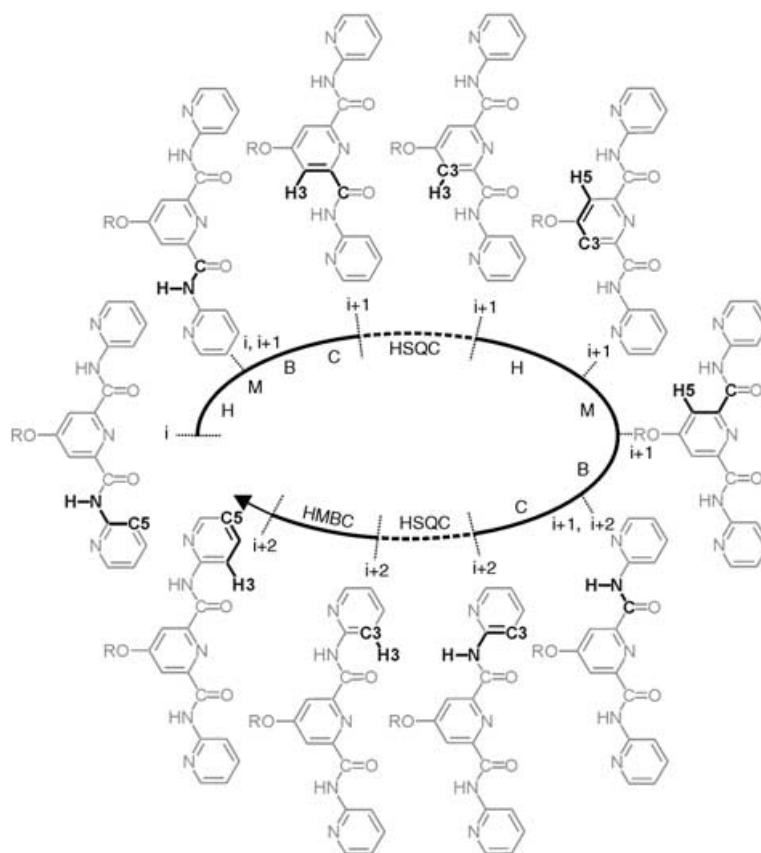


Figure 5. Schematic representation of HSQC and HMBC correlations which allow to connect residue i to residue $i+2$ in tridecamer **2**.

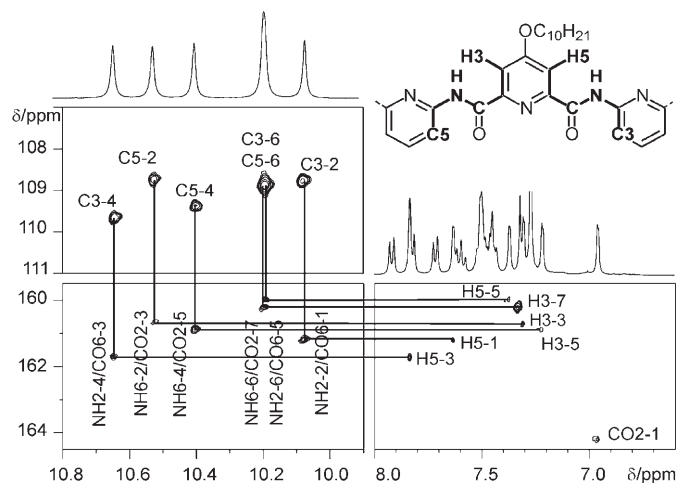


Figure 6. Parts of the 400 MHz HMBC plot of **2** in CDCl₃ at 300 K, showing cross-peaks between carbons C5 and C3 and amide protons (top), between amide protons and carbonyl carbons (bottom left), and between carbonyl and protons H3 and H5 (bottom right) used for sequence assignment to go from residue *i* to residue *i*+2. The horizontal scale is that of proton resonances and the vertical scale is that of carbon resonances.

carbon CO-1 is 164.1 ppm whilst other carbonyls are found between 160.0 and 161.5 ppm.

These experiments have allowed to assign the signals of all aromatic and amide protons and carbons in **1** and **2**. Two tables giving this full assignment and the correlations observed between them can be found in the Supporting Information. Of course, the presence of C₂-symmetry axis in **2** causes all signals to be degenerate and to belong to two equivalent protons at different positions of the strand.

An interesting observation that can be made from this assignment concerns the variation of the amide resonances as a function of their position in the sequence (Figure 7). Both for **1** and **2**, the most shielded amide protons are the ones at the core of the sequence, and also the ones at the extremities. The shielding of the protons at the core of the sequence is not surprising since they are sandwiched between aromatic rings. The chemical shift of the peripheral amide protons may arise from a higher conformational mobility at the

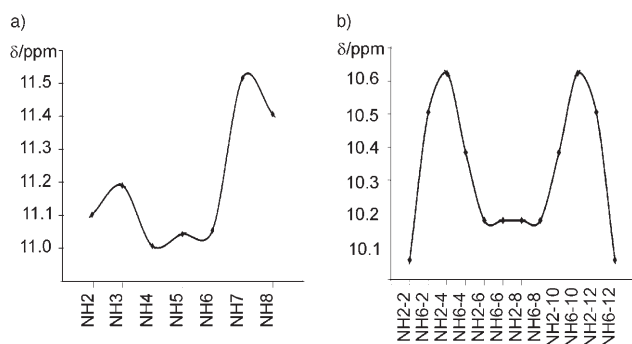


Figure 7. Variation of chemical shift of amide protons with their position in the sequence for a) octamer **1** and b) tridecamer **2**. The line is for guiding the eye only.

strands extremities and thus a weaker effect of the deshielding associated with intramolecular hydrogen bonding.

Determination of the conformations: Determinations of the structures were carried out with NMR ¹H/¹H ROESY experiments. Many attempts were first performed by using NOESY experiments, but in the range of molar masses of both compounds, NOE correlation signals have the same phase as the diagonal signals, and so cross-peaks can hardly be distinguished from other correlations, TOCSY for instance, or noise. The ROESY experiment is more effective in our case, since the phase of the diagonal signals is the same as TOCSY breakthrough signals, and NOE correlations are in anti-phase.

The regions of the ROESY plot of octamer **1** containing important data concern aromatic, side chain OCH₂, amide and ester resonances. Aromatic proton H3 from a residue *i* shows up to six NOE correlations with aromatic protons H5, H6 and H7 from residues *i*+3 and *i*-2 (Figure 8a). Of course, H3 protons in residues 1 and 2 correlate only with protons in residue 4 and 5, respectively, and H3 protons of residues 6, 7 and 8 only correlate with protons in residues 4, 5 and 6, respectively. Interestingly, the OCH₂ protons of a residue *i* (which can be identified through an NOE correlation with the nearby proton H3) show the same NOE correlations with aromatic protons H5, H6 and H7 from residues *i*+3 and *i*-2. The signals of OCH₂ protons show diastereotopic patterns, except those of residues 6, 7 and 8 at the C-terminus. The methyl ester protons show a single correlation with aromatic proton H3-6 (Figure 8b). The intensity of this cross-peak is one of the strongest observed on the ROESY spectra; the proton-proton distance is thus one of the shortest. In the region of amide resonances, the signal of the amide of residue *i* shows cross-peaks with the signals of amides residues *i*-2, *i*-1, *i*+1 and *i*+2 (Figure 8c). Most of these numerous NOE correlations are schematized in Figure 8e. They are all consistent with a helical structure of octamer **1**.

NOE correlations were more difficult to identify for tridecamer **2** because of the C₂ symmetry of the strand, and because of the overlap between aromatic ¹H NMR signals. The regions of the ROESY plot containing important data again concern aromatic and amide proton resonances. NOE correlations between aromatic protons overlap too much and are too weak to be distinguished from TOCSY correlations or noise. Fortunately, in the region of amide resonances, five cross-peaks are well-defined, two with weak intensity and three with high intensity (Figure 8d). As shown in Figure 9, these five cross-peaks are consistent with the helical structure observed in the crystal of analogues of **2**. The three stronger cross-peaks can be assigned to correlations between amide protons following each other in the sequence (*i*, *i*+2); they arise from the close distance between the two protons of a 2,6-pyridinedicarboxamide unit (Figure 8f). Of course, the symmetry of the oligomer and degeneracy of the signal allows other assignments, but these would be incompatible with the helical structure observed in the crystal

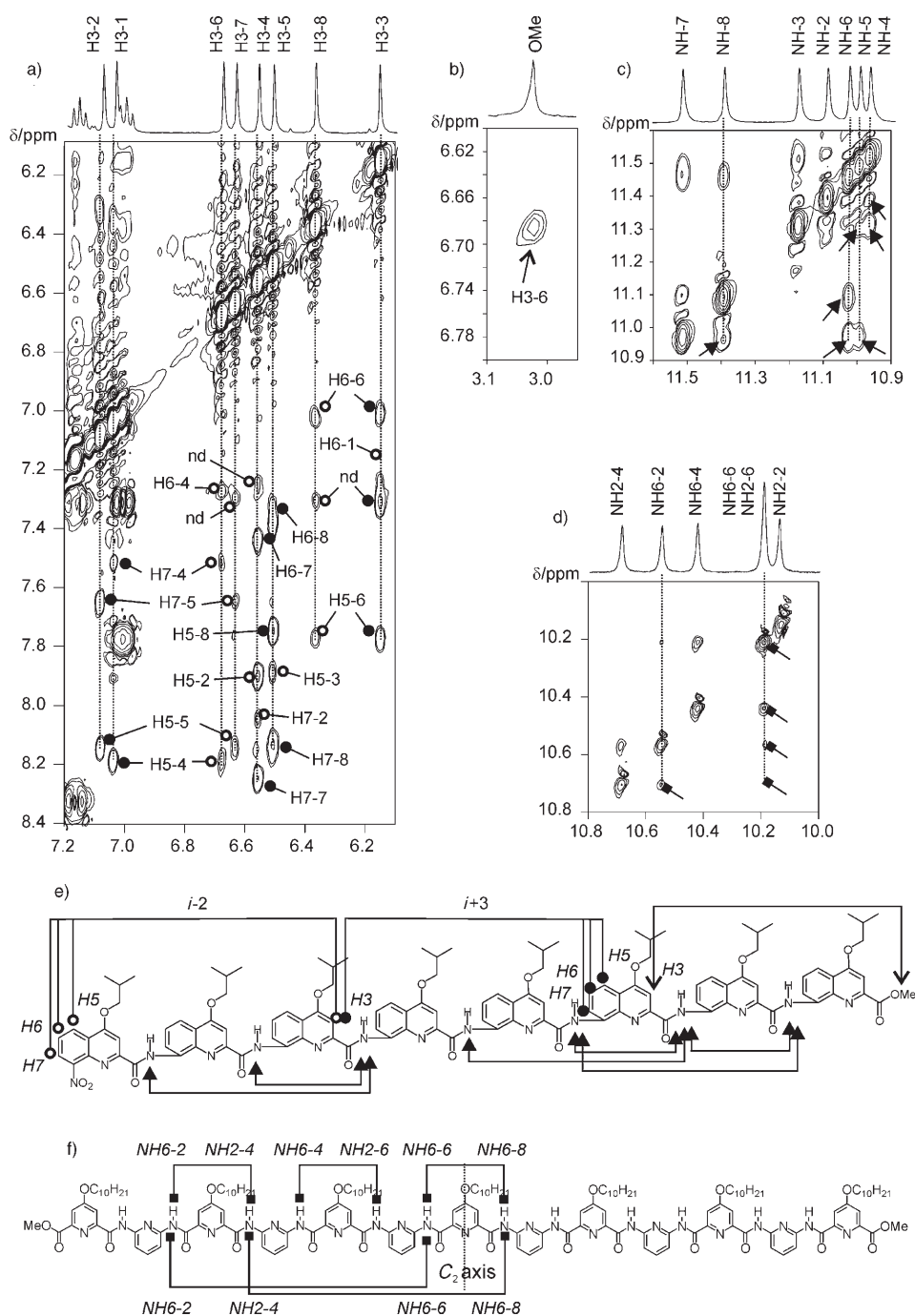


Figure 8. Parts of the 400 MHz ROESY plots ($\tau_m=300$ ms) of **1** and **2** showing cross-peaks between a) aromatic protons in **1**; b) ester and aromatic protons in **1**; c) amide protons in **1**; d) amide protons in **2**. Structures of e) octamer **1** and f) tridecamer **2** summarizing NOE correlations identified from ROESY spectra. \circ and \bullet in charts a) and e) represent correlations between a proton in residue i and protons in residues $i-2$ and $i+3$, respectively. A few unassigned correlations are labeled "nd".

(Figure 9). The two weaker correlations occur between protons more remote from each other in the sequence (ring i and ring $i+4$). Again, other possible assignments are not consistent with the helical structure observed in the crystal.

Due to the low number of NOE correlations in tridecamer **2**, molecular modeling calculations were not attempted.

The main obstacle to a full analysis of this structure is the overlap between aromatic signals. Full assignment of the sequence was possible; however, we could not fully assign the ROESY spectrum. Measurements at higher field (e.g. 600 MHz with a cryoprobe) may be attempted in the future.

The conformation of octamer **1** in solution was further investigated by restrained molecular dynamics calculations. Distance constraints were extracted from the ROESY spectrum. NOE correlations which could not be assigned unambiguously because of NMR signals overlap were not used in structure calculations. Inter-proton distances for octamer **1** were obtained by measuring cross-peaks volumes in the ROESY spectra, taking as a reference a distance of 2.3 Å between the proton H3 of each quinoline ring and the diastereotopic OCH₂ protons of the same ring. Distance restraints were assigned as strong, medium and weak, and set at intervals of 2.2 ± 0.4 , 3.5 ± 0.9 and 5 ± 0.6 Å, respectively. Structures were calculated from 30 inter-residue NOE (distance constraints) using the MM3* force field in the MacroModel program, by using a fully extended conformation of the oligomer as well as a helical conformation as starting structures. Monte Carlo-style conformational search was also performed with the fully extended conformation as starting structure. All simulations converged towards helical structures each time, with MM3*, regardless of the starting structure. The superimposition of the 10 lowest energy structures (Figure 10a)

showed that the helical backbone is well-defined. Some disorder around isobutyl chains in position 4 of the quinoline rings reveals the flexibility of these substituents. Overlay of the lowest energy structure and the crystal structure (Figure 10b) reveals a very similar backbone conformation in solution and in the solid-state. The slight discrepancies be-

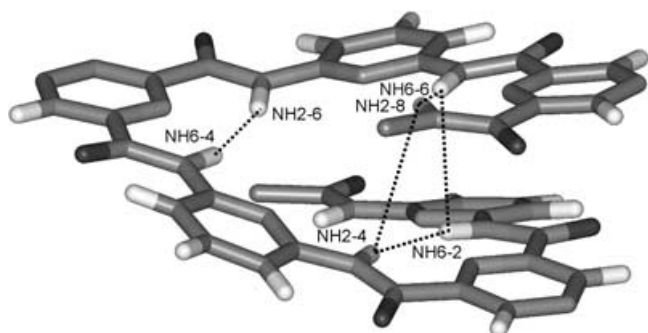


Figure 9. Part of the crystal structure of an analogue of **2** showing the five correlations observed in the 400 MHz ROESY plot of **2** (dotted lines). These correlations are consistent with the distances observed in the crystal: $d(\text{NH6-4-NH2-6}) = 2.61 \text{ \AA}$; $d(\text{NH6-6-NH2-8}) = 2.81 \text{ \AA}$; $d(\text{NH6-2-NH2-4}) = 2.59 \text{ \AA}$; $d(\text{NH6-2-NH6-6}) = 3.24 \text{ \AA}$; $d(\text{NH2-4-NH2-8}) = 3.45 \text{ \AA}$.

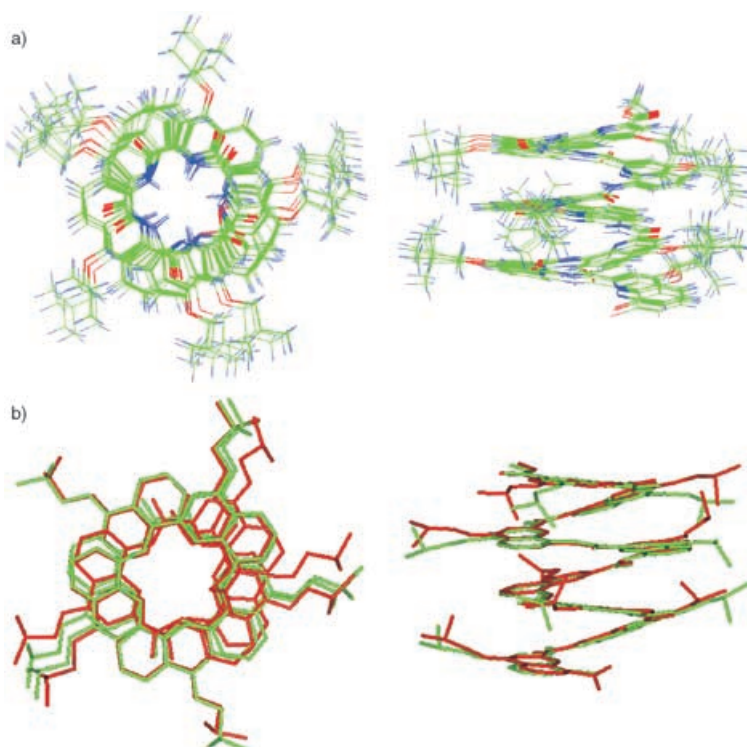


Figure 10. a) Side view and top view of superimposed ten lowest energy structures of **1** obtained from restrained stochastic dynamic simulations at 1000 K with a helical conformation used as a starting structure. b) Superimposition of the lowest energy calculated structure and of the crystal structure. Root-mean-square (RMS) differences of bond and angle deviations from the crystal structure were 0.377 \AA and 3° , respectively.

tween the crystal structure and the energy minimized structures might reflect minor but genuine differences between solid state conformation and solution conformations. More likely, these differences originate from imperfections in the force field parameters.

Conclusion

The NMR protocols developed for solving the solution structures of α -peptides have been applied to aliphatic β - and γ -peptides but are not directly applicable to aromatic oligomers. In particular, the string of spin systems in an aromatic sequence cannot be reconstituted solely from correlations between protons. We have shown that the assignment of a large part of the ^{13}C NMR spectrum through HMBC and HSQC experiments allows to unambiguously assign the proton NMR spectrum. This has been implemented both with quinoline- and pyridine-derived oligoamide foldamers, and should be applicable to a wide range of oligomers including various combinations of monomers. This assignment in turns allows for the interpretation of NOE correlations and, when enough distance constraints can be obtained, to

the direct determination of the solution structure. The full assignment also paves the way to other types of NMR experiments, for example the investigation of dynamic phenomena within the oligomer. For aza-aromatic oligoamides, the structures obtained in solution correspond very well with those observed in the solid state. In the pyridine series, overlap between aromatic signals still comes as a limitation to interpret NOE correlations. However, it should be emphasized that the oligomers studied here are highly repetitive sequences, and also that the instrumentation used - a simple 400 MHz spectrometer - is relatively standard. More advanced instrumentation should allow to fully solve even more complicated cases.

Experimental Section

NMR Spectroscopy

General methods: Spectra were recorded with a Bruker Avance 400 NB US NMR spectrometer by means of a

5 mm direct QNP 1H/X probe with gradient capabilities. The temperature was maintained at 300 K for the structure determination. ^1H , ^{13}C , double quantum filtered correlated spectroscopy (DQF-COSY),^[19] heteronuclear single quantum coherence (HSQC),^[20] heteronuclear multiple bond correlation (HMBC),^[21] and rotating frame nuclear Overhauser spectroscopy (ROESY),^[22] spectra were used for sequence-specific assignments of both compounds. Data processing was performed with XWIN-NMR software.

Sample preparation: The synthesis of octamer **1** was described previously.^[14b] The synthesis of tridecamer **2** was performed by using published procedures.^[16,23] NMR samples were prepared by dissolving the solids in

CDCl_3 (0.5 mL) to reach a concentration of 5 mM for **1** and of only 2 mM for **2** to avoid its hybridization into double helices.^[16,17]

Octamer 1: The DQF-COSY was performed by a gradient-selection pathway. Acquisition with $512(t_2) \times 256(t_1)$ data points; relaxation delay of 2 s; sweep width of 1000 Hz in both dimensions; QF mode in t_1 and eight scans per increment. Processing was done after a sine-bell multiplication in both dimensions, and Fourier transformed in $1 \text{ k} \times 1 \text{ k}$ real data points.

The HSQC acquisition was performed with $1024(t_2) \times 512(t_1)$ data points in echo-antiecho mode with Z gradients selection; a relaxation delay of 2 s and 32 scans per increment; and a sweep width of 4800 Hz for the proton dimension and 17000 Hz for the carbon dimension. Processing was done after a cosine multiplication in both dimensions, and Fourier transformed in $1 \text{ k} \times 1 \text{ k}$ real data points.

The HMBC acquisition was performed with $1024(t_2) \times 512(t_1)$ data points in QF mode in t_1 with Z gradients selection; a relaxation delay of 2 s and 40 scans per increment; and a sweep width of 4800 Hz for the proton dimension and 17000 Hz for the carbon dimension. Processing was done after a cosine multiplication in both dimensions, and Fourier transformed in $1 \text{ k} \times 1 \text{ k}$ real data points.

The ROESY acquisition was performed with $1024(t_2) \times 256(t_1)$ data points in States-TPPI mode with Z gradients selection and with CW-spin lock for mixing; a relaxation delay of 2 s and 64 scans per increment; a sweep width of 3400 Hz in both dimensions; and a mixing time of 300 ms. Processing was done after a sine-bell multiplication in both dimensions, and Fourier transformed in $1 \text{ k} \times 1 \text{ k}$ real data points.

Tridecamer 2: The DQF-COSY was performed by a gradient-selection pathway. Acquisition with $256(t_2) \times 256(t_1)$ data points; relaxation delay of 2 s; sweep width of 800 Hz in both dimensions; QF mode in t_1 and one scan per increment. Processing was done after a sine-bell multiplication in both dimensions, and Fourier transformed in $1 \text{ k} \times 1 \text{ k}$ real data points.

The HSQC acquisition was performed with $1024(t_2) \times 256(t_1)$ data points in echo-antiecho mode with Z gradients selection; a relaxation delay of 2 s and 64 scans per increment; and a sweep width of 4400 Hz for the proton dimension and 18000 Hz for the carbon dimension. Processing was done after a cosine multiplication in both dimensions, and Fourier transformed in $1 \text{ k} \times 1 \text{ k}$ real data points.

The HMBC acquisition was performed with $1024(t_2) \times 256(t_1)$ data points in QF mode in t_1 with Z gradients selection; a relaxation delay of 2 s and 78 scans per increment; and a sweep width of 4400 Hz for the proton dimension and 18000 Hz for the carbon dimension. Processing was done after a cosine multiplication in both dimensions, and Fourier transformed in $1 \text{ k} \times 1 \text{ k}$ real data points.

The ROESY acquisition was performed with $512(t_2) \times 512(t_1)$ data points in States-TPPI mode with Z gradients selection and with CW-spin lock for mixing; a relaxation delay of 2 s and 32 scans per increment; a sweep width of 640 Hz in both dimensions and a mixing time of 300 ms. Processing was done after a sine-bell multiplication in both dimensions, and Fourier transformed in $1 \text{ k} \times 1 \text{ k}$ real data points.

Molecular modeling calculations

General: Restrained molecular modeling calculations for octamer **1** were performed on a R10 000 O2 Silicon Graphics workstation using MacroModel version 6.5 (Schrödinger Inc.). Conformational minima were found using the modified MM3* (1991 parameters) force field as implemented and completed in the MacroModel program. Build structures were minimized to a final RMS gradient $\leq 0.005 \text{ kJ } \text{Å}^{-1} \text{ mol}^{-1}$ by the truncated newton conjugate gradient (TNCG) method (1000 cycles). In all cases the extended cut-off option was used throughout ($\text{VdW} = 8 \text{ Å}$, electrostatic = 20 Å and hydrogen bond = 4 Å).

Extraction of distance constraints from 2D ROESY spectra: Interproton distances for octamer **1** were obtained by measuring cross-peak volumes in the ROESY spectra, taking as a reference the distance of 2.3 Å between the proton H_3 of the quinoline ring and the diastereotopic protons OCH_2 in position 4. Distance restraints were assigned as strong, medium and weak, and set at intervals of 2.2 ± 0.4 , 3.5 ± 0.9 and $5 \pm 0.6 \text{ Å}$, respectively. For this purpose a flat-bottomed well potential was used.

Stochastic dynamic simulations: Stochastic dynamic simulations were accomplished using the variant of molecular dynamics that is implemented in MacroModel. The forces from the force field were augmented by frictional and random forces that simulate some properties of a solvent medium.^[24] Two runs were performed with a fully extended conformation and a helical conformation used as starting structures. The chosen temperature was 1000 K, the time step was 1.0 fs, the total simulation time in each case was 5 ns and 500 snapshots were saved for each run. All saved conformers were fully minimized without constraints and ranked by ascending energy (TNCG, 1000 steps). The final 20 structures with the lowest energy were used for the structural analysis.

Monte Carlo-style conformational search: This search is implemented in MacroModel.^[25,26] The manual setup was selected, that is, the 14 single bonds corresponding to the junction between the amide function and the aromatic rings were kept flexible. In order to insure convergence 1000 steps were made per input structure, in an energy range of 20 kJ mol^{-1} (solution accessible conformation). The same constraint set as above was used throughout. Each conformer was fully minimized (1000 cycles, TNCG method, $\text{RMS} \leq 0.005 \text{ kJ } \text{Å}^{-1} \text{ mol}^{-1}$, MM3* force field). The least-used structures were used as starting geometries only if their energies were within the energetic window (20 kJ mol^{-1} of the lowest energy structure yet found). Afterwards the 186 conformers found at this stage were re-minimized, unconstrained, leading to a final set of 54 conformers. The Insight II program (Accelrys Inc.) was used for structural analysis of the different obtained conformations.

Acknowledgements

This work was supported by the CNRS, the Conseil Régional d'Aquitaine (predoctoral fellowships to C.D. and V.M.) and by the French Ministry of research (post-doctoral fellowship to H.J.).

- [1] For reviews, see: a) D. J. Hill, M. J. Moi, R. B. Prince, T. S. Hughes, J. S. Moore, *Chem. Rev.* **2001**, *101*, 3893–4011; b) C. Schmuck, *Angew. Chem.* **2003**, *115*, 2552–2556; *Angew. Chem. Int. Ed.* **2003**, *42*, 2448–2452; c) I. Huc, *Eur. J. Org. Chem.* **2004**, 17–29.
- [2] For reviews, see: D. Seebach, A. K. Beck, D. J. Bierbaum, *Chem. Biodiversity* **2004**, *1*, 1111–1239; G. Guichard in *Pseudo-Peptides in Drug Discovery* (Ed.: P. E. Nielsen), Wiley-VCH, Weinheim, **2004**, pp. 33–120; R. P. Cheng, S. H. Gellman, W. F. DeGrado, *Chem. Rev.* **2001**, *101*, 3219–3232; G. Licini, L. J. Prins, P. Scrimin, *Eur. J. Org. Chem.* **2005**, 969–977.
- [3] For examples, see: D. Liu, S. Choi, B. Chen, R. J. Doerksen, D. J. Clements, J. D. Winkler, M. L. Klein, W. F. DeGrado, *Angew. Chem.* **2004**, *116*, 1178–1182; *Angew. Chem. Int. Ed.* **2004**, *43*, 1158–1162; J. A. Patch, A. E. Barron, *J. Am. Chem. Soc.* **2003**, *125*, 12092–12093; N. Umezawa, M. A. Gelman, M. C. Haigis, R. T. Raines, S. H. Gellman, *J. Am. Chem. Soc.* **2002**, *124*, 368–369; E. Porter, B. Weisblum, S. H. Gellman, *J. Am. Chem. Soc.* **2002**, *124*, 7324–7330; E. Porter, X. Wang, H.-S. Lee, B. Weisblum, S. H. Gellman, *Nature* **2000**, *404*, 565; M. Werder, H. Hauser, S. Abele, D. Seebach, *Helv. Chim. Acta* **1999**, *82*, 1774–1783; Y. Hamuro, J. P. Schneider, W. F. DeGrado, *J. Am. Chem. Soc.* **1999**, *121*, 12200–12201.
- [4] R. B. Prince, S. A. Barnes, J. S. Moore, *J. Am. Chem. Soc.* **2000**, *122*, 2758–2762; T. Nishinaga, A. Tanatani, O. Keuchan, J. S. Moore, *J. Am. Chem. Soc.* **2002**, *124*, 5934–5935; A. Tanatani, T. S. Hughes, J. S. Moore, *Angew. Chem.* **2002**, *114*, 335–338; *Angew. Chem. Int. Ed.* **2002**, *41*, 325–328; M. T. Stone, J. S. Moore, *Org. Lett.* **2004**, *6*, 469–472.
- [5] M. Inouye, M. Waki, H. Abe, *J. Am. Chem. Soc.* **2004**, *126*, 2022–2027.
- [6] J.-L. Hou, X.-B. Shao, G.-J. Chen, Y.-X. Zhou, X.-K. Jiang, Z.-T. Li, *J. Am. Chem. Soc.* **2004**, *126*, 12386–12394; J.-L. Hou, M.-X. Jia, X.-K. Jiang, Z.-T. Li, G.-J. Chen, *J. Org. Chem.* **2004**, *69*, 6228–6237.
- [7] J. Garric, J.-M. Léger, I. Huc, *Angew. Chem.* **2005**, *117*, 1990–1994; *Angew. Chem. Int. Ed.* **2005**, *44*, 1954–1958.

- [8] A. Glattli, X. Daura, D. Seebach, W. F. van Gunsteren, *J. Am. Chem. Soc.* **2002**, *124*, 12972–12978.
- [9] For example: V. Semetey, D. Rognan, C. Hemmerlin, R. Graff, J.-P. Briand, M. Marraud, G. Guichard, *Angew. Chem.* **2002**, *114*, 1973–1975; *Angew. Chem. Int. Ed.* **2002**, *41*, 1893–1895; D. Seebach, Y. R. Mahajan, R. Senthilkumar, M. Rueping, B. Jaun, *Chem. Commun.* **2002**, 11836–11837; P. R. LePlae, J. D. Fisk, E. A. Porter, B. Weisblum, S. H. Gellman, *J. Am. Chem. Soc.* **2002**, *124*, 6820–6821; H.-S. Lee, F. A. Syud, X. Wang, S. H. Gellman, *J. Am. Chem. Soc.* **2001**, *123*, 7721–7722; J. J. Barchi, Jr., X. Huang, D. H. Appella, L. A. Christianson, S. R. Durell, S. H. Gellman, *J. Am. Chem. Soc.* **2000**, *122*, 2711–2718.
- [10] S. Mammi, M. Rainaldi, M. Bellanda, E. Schievano, E. Peggion, Q. B. Broxterman, F. Formaggio, M. Crisma, C. Toniolo, *J. Am. Chem. Soc.* **2000**, *122*, 11735–11736.
- [11] R. B. Prince, J. G. Saven, P. G. Wolynes, J. S. Moore, *J. Am. Chem. Soc.* **1999**, *121*, 3114–3121.
- [12] G. J. Gabriel, S. Sorey, B. L. Iverson, *J. Am. Chem. Soc.* **2005**, *127*, 2637–2640; L. Yuan, H. Zeng, K. Yamato, A. R. Sanford, W. Feng, H. S. Atreya, D. K. Sukumaran, T. Szyperski, B. Gong, *J. Am. Chem. Soc.* **2004**, *126*, 16528–16537.
- [13] K. Matsuda, M. T. Stone, J. S. Moore, *J. Am. Chem. Soc.* **2002**, *124*, 11836–11837.
- [14] a) H. Jiang, J.-M. Léger, I. Huc, *J. Am. Chem. Soc.* **2003**, *125*, 3448–3449; b) H. Jiang, J.-M. Léger, C. Dolain, P. Guionneau, I. Huc, *Tetrahedron* **2003**, *59*, 8365–8374; c) H. Jiang, C. Dolain, J.-M. Léger, H. Gornitzka, I. Huc, *J. Am. Chem. Soc.* **2004**, *126*, 1034–1035; d) V. Maurizot, C. Dolain, Y. Leydet, J.-M. Léger, P. Guionneau, I. Huc, *J. Am. Chem. Soc.* **2004**, *126*, 10049–10052.
- [15] V. Berl, I. Huc, R. Khoury, J.-M. Lehn, *Chem. Eur. J.* **2001**, *7*, 2798–2809; I. Huc, V. Maurizot, H. Gornitzka, J.-M. Léger, *Chem. Commun.* **2002**, 578–579.
- [16] V. Berl, I. Huc, R. G. Khoury, M. Krische, J.-M. Lehn, *Nature* **2000**, *407*, 720–723; V. Berl, I. Huc, R. G. Khoury, J.-M. Lehn, *Chem. Eur. J.* **2001**, *7*, 2810–2820; V. Maurizot, J.-M. Léger, P. Guionneau, I. Huc, *Russ. Chem. Bull.* **2004**, *53*, 1572–1576.
- [17] H. Jiang, V. Maurizot, I. Huc, *Tetrahedron* **2004**, *60*, 10029–10038.
- [18] See Supporting Information.
- [19] R. R. Ernst, *Chem. Phys. Lett.* **1977**, *52*, 407–412; B. Ancian, I. Bourgeois, J.-F. Dauphin, A. A. Shaw, *J. Magn. Reson.* **1997**, *125*, 348–354.
- [20] A. G. Palmer III, J. Cavanagh, P. E. Wright, M. Rance, *J. Magn. Reson.* **1991**, *93*, 151–170; L. E. Kay, P. Keifer, T. Saarinen, *J. Am. Chem. Soc.* **1992**, *114*, 10663–10665; J. Schleucher, M. Schwendinger, M. Sattler, P. Schmidt, O. Schedletsky, S. J. Glaser, O. W. Sorensen, C. Griesinger, *J. Biomol. NMR* **1994**, *4*, 301–306.
- [21] A. Bax, M. J. Summers, *J. Am. Chem. Soc.* **1986**, *108*, 2093–2094.
- [22] A. Bax, D. G. Davis, *J. Magn. Reson.* **1985**, *63*, 207–213.
- [23] V. Maurizot, C. Dolain, I. Huc, *Eur. J. Org. Chem.* **2005**, *7*, 1293–1301.
- [24] W. F. Van Gunsteren, H. J. C. Berendsen, *J. Comput.-Aided Mol. Des.* **1987**, *1*, 171–176.
- [25] G. Chang, W. C. Guida, W. C. Still, *J. Am. Chem. Soc.* **1989**, *111*, 4379–4386.
- [26] M. Saunders, K. N. Houk, Y. D. Wu, W. C. Still, M. Lipton, G. Chang, W. C. Guida, *J. Am. Chem. Soc.* **1990**, *112*, 1419–1427.

Received: April 7, 2005
Published online: August 1, 2005